PIV measurements in a real time controlled model wind turbine wake simulator

R Castillo[1], Y Wang[1], T Monk[1], S Vasquez[1], S Pol[1], B Ren[1], A Swift[1], F Hussain[1] and C H Westergaard[1]

[1]Texas Tech University, Lubbock, TX, USA
email: suhas.pol@ttu.edu

Abstract. A wind tunnel based "Hyper Accelerated Wind Farm Kinematic-Control Simulator" (HAWKS) is being built at Texas Tech University (TTU) to emulate controlled wind turbine flow physics. The HAWKS model turbine has pitch, yaw and speed controls that could be operated in real time with different power coefficient (C_P) conditions. The purpose of HAWKS is to simulate control strategies, operating at much faster turnaround times. Currently, the fundamental building blocks of the simulator are being tested. A few salient tests results are presented here.

1. Introduction

Wind turbine wake control as a strategy to improve wind farm output has been researched so far for specific array configurations considering only steady state conditions [1-6]. However, fast dynamic changes in speed and pitch angle corresponding to yaw input should be considered given the inherent unsteady nature of the incoming turbulent inflow. Using high fidelity CFD tools for changing control parameters requires substantial computational resources and time [8, 9]. Exploring innovative strategies in full scale turbines is impractical and expensive, and may not be available for iterative development of wake control strategies.

To emulate the full scale physics of closed loop control based on changes in real time (with respect to a high rotor speed) a "Hyper Accelerated Wind Farm Kinematic-Control Simulator" (HAWKS) is being built at Texas Tech University (TTU). The HAWKS will measure wake characteristics which then provide input to the turbine controller producing the desired downstream effects. HAWKS aims at being a platform to test wake steering control strategies to improve wind turbine array output. HAWKS results will be implemented eventually at the DOE/Sandia SWiFT facility [11]. This facility will be augmented with multiple ground based and downstream facing nacelle mounted LIDAR installations to characterize the wake.

This paper describes the capabilities of the HAWKS platform and shows the preliminary results with the capabilities developed so far. The experimental setup is described in section 2. An analysis of the test results is presented in section 3. The plan to expand HAWKS to a model wind farm is described in section 4.

2. Experimental Setup

The study was carried out in a closed loop wind tunnel of 1.2m x 1.8m cross-section with a uniform inflow velocity, U_∞ =10.85 m/s. A single fully controllable 3 bladed horizontal axis wind turbine model of diameter, D=0.26m was deployed for the study. The rotor has straight, 0.013m constant chord blades with an airfoil profile matching NACA 0012. To test the HAWKS concept feasibility, the blades and pitch control hardware of model RC helicopter were used. The aerodynamic performance of this rotor

was satisfactory and is presented in section 3. A 15W AMETEK 8693S039-SP DC motor that performed as a generator was enclosed in a nacelle of 0.07m x 0.038m cross section and 0.13m length.

Controlling the rotor speed, pitch and yaw angle are important capabilities of the HAWKS to achieve multi-level operating conditions. The rotor speed is controlled by adjusting the duty cycle of the DC-DC buck converter. The blade pitch angle is controlled collectively by a set of 3 actuators and ranges from 0 to 24° in steps of 0.3° at a rate of 4°/rev. The yaw system is driven by a servomotor Futaba S9155, whose rotation angle corresponds to the actual wind turbine yaw angle, at a rate of 4°/rev. Both the yaw and pitch actuators are coupled to a Texas Instrument TMS320F28335 microcontroller.

Particle Image Velocimetry (PIV) technique was employed to measure the velocity distribution across a planar area of the flow field downstream of the turbine. A 150 mJ/pulse Nd:YAG laser coupled with laser sheet forming optics was used to illuminate the flow seeded by a particle generator using propylene glycol oil droplets. The particle images were recorded with an array of four 14-bit La Vision CCD cameras with a resolution of 1600 x 1200 pixels each using 50 mm lens that were synchronized with the laser pulses. The CCD cameras were 2.2 m away from the light sheet plane, so that the image yielded a total inspection area of about 1.4D x 7.5D. The image resolution was 3.2 pixels/mm. The schematic of the PIV setup as well as the axis definition in the test section are shown in figure 1.

The images were processed using standard La Vision software. The size of the interrogation window in the correlation calculation was 32x32 pixels with an overlap of 50%, resulting in a vector resolution of 1 per 5 mm.

Due to the configuration of the wind tunnel, the PIV setup shown in figure 1 allows us to measure the velocity distribution in a plane parallel to the lateral walls of the tunnel. In order to measure the velocity distribution at hub height, the wind turbine was rotated 90° attaching the tower to one of the wind tunnel lateral walls. The turbine hub was located at the center of the tunnel in the cross stream direction, and 0.44 m above the floor.

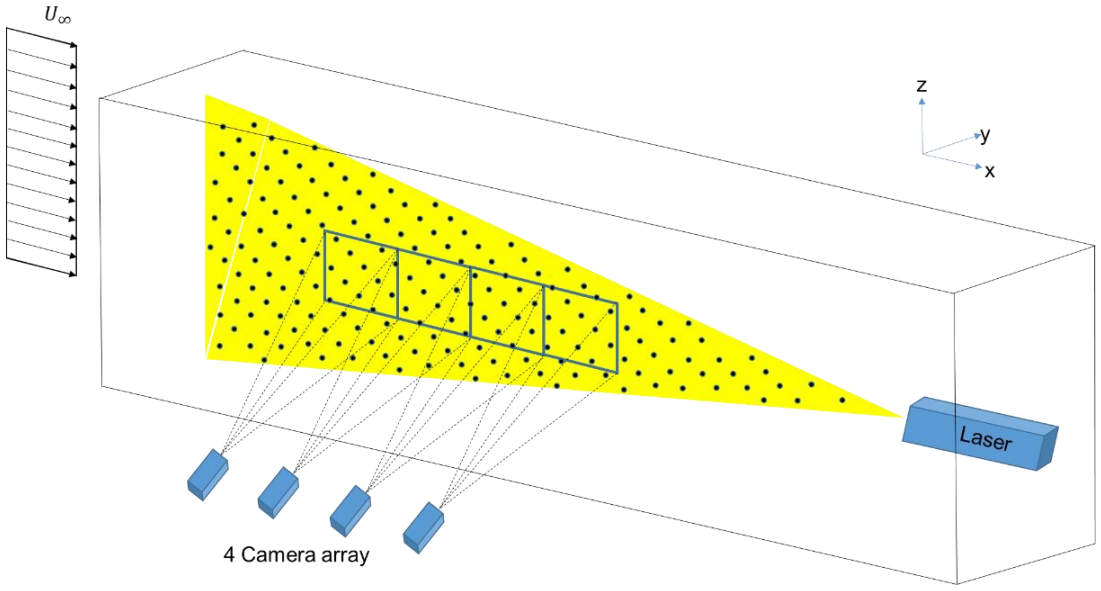

Figure 1. Schematic of the HAWKS PIV system and the test section.

3. Test Results

This section outlines the preliminary results of the tests performed in the HAWKS platform, where the model turbine performance and its wake characteristics were measured and analyzed under various static yaw conditions. In addition to exploring the possibility of controlling the wake under dynamic yaw conditions, preliminary wake velocity measurements for a dynamic yaw case are also presented.

3.1. Effect of yaw misalignment on turbine performance

One of the key factors that determines the turbine performance is the power coefficient (C_P), which is a function of the tip speed ratio (λ), blade pitch angle (β) and yaw misalignment (δ). For δ=0, the power coefficient $C_P(\lambda, \beta)|_{\delta=0}$ of the model wind turbine was characterized by adjusting the electrical load at different pitch angles. The optimal power coefficient, $C_P|_{\delta=0,\lambda=\lambda_{opt}}$ was approximately 0.27 and occurred at β_{opt}=6° and λ_{opt}=7, when the electrical load was Ω=19 ohms.

To observe the influence of yaw misalignment on the turbine C_P, eleven different yaw angles were considered, from -25° to 25° with a 5° increment. The yaw angle followed the convention defined in [5], where δ is positive when the later component of the inflow with respect to the rotor disc is in the same direction as the blade movement when the blade is at the top dead center.

For each yaw angle, the pitch angle (β=6°), the electrical load on the generator (Ω=19 ohms) and the wind speed (U_∞ =10.85 m/s) were held constant, and the rotor speed, output voltage and current were measured to calculate the C_P. A reduction in rotor speed and hence in λ was observed with increasing δ. As a consequence, C_P changed due to both λ and δ. To isolate the $C_P(\lambda, \delta)$ variation exclusively due to δ at $\lambda=\lambda_{opt}$, a correction was applied such that

$$C_P(\delta)|_{\lambda=\lambda_{opt}} = \frac{\left(C_P(\lambda,\delta)\right)\left(C_P|_{\delta=0,\lambda=\lambda_{opt}}\right)}{C_P(\lambda)|_{\delta=0}} \qquad (1)$$

where λ_{opt} is the optimal tip speed ratio at δ=0, and $C_P(\lambda)|_{\delta=0}$ is the C_P value as a function of λ at δ=0. The corrected C_P for each yaw angle case $C_P(\delta)|_{\lambda=\lambda_{opt}}$ is shown in figure 2. For a yawed turbine, the power generated follows a $\cos^n(\delta)$ relationship, where n=2 or 3 depending on the study [3]. Based on our measurements, $C_P(\delta)|_{\lambda=\lambda_{opt}}$ follows a $\cos^2(\delta)$ relationship. Further, the variation of C_P in figure 2 is not sensitive to yaw direction, since the C_P curve appears symmetrical with δ about δ=0°. This observation is in qualitative agreement with measurements presented in figure 4 of Ref [12] and other literature such as Refs. [3, 5]. Since wake deflection control is current research priority, this analysis was not pursued further.

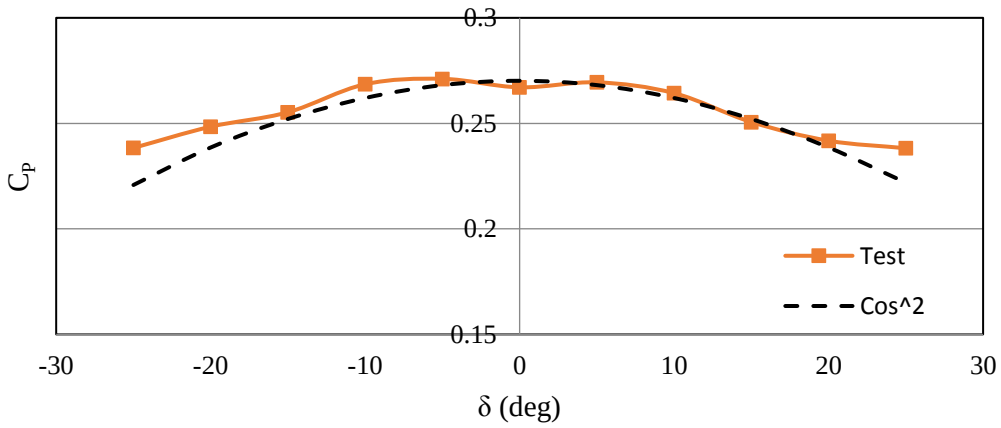

Figure 2. Comparison between C_P corrected from HAWKS test and C_P following a $\cos^2(\delta)$ relationship.

3.2. Wake characteristics under Static yaw

For each of the above yaw cases, a set of 500 images were recorded (equivalent to 50 seconds). The recorded images correspond to a horizontal plane at hub height. The instantaneous velocity vector fields were calculated using Davis software from background subtracted raw images (see section 2 for setting details). The instantaneous streamwise velocity was averaged and normalized by the uniform

inflow velocity ($\overline{U}/U_\infty$). The resulting contours are shown in figure 3. The quality of the contours was affected by some features at x/D=5.5 and 6.5 as a consequence of damaged pixels on the cameras. However, the contours qualitatively show that the wake deflects for each static yaw case.

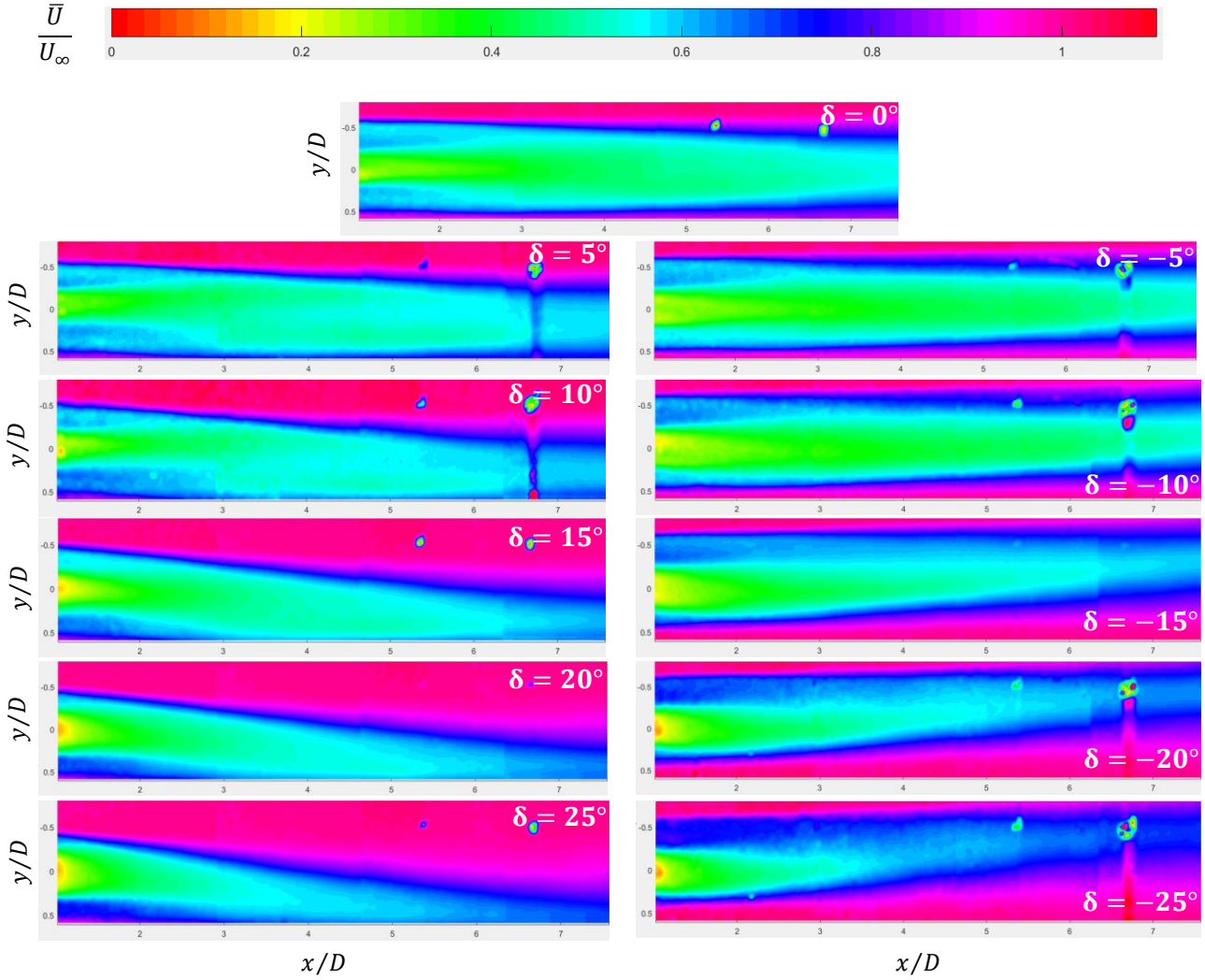

a) b)

Figure 3. Contours of the normalized mean streamwise velocity ($\overline{U}/U_\infty$) in the horizontal plane at hub height for increasing different yaw angles. Column a) Positive (+) yaw. Column b) Negative (-) yaw

Figure 4 compares normalized mean streamwise velocity profiles across the wake at various downstream distances for different static yaw cases specified above. The velocity profile for the δ=0° case is, not surprisingly, symmetrical about the center of the rotor y/D=0. However, for the yawed cases, the profile becomes asymmetrical as the wake is deflected to a side. The degree of asymmetry and hence the wake deflection increases with the yaw angle. Figure 4a shows that the central part of the near wake region is considerably influenced by the shape and size of the nacelle, a consequence of its large frontal area. Further, the effective frontal area increases with yaw angle leading to larger wake deficit than usual. Figure 4b to 4d show that the far wake region is less sensitive to the nacelle dimensions, as expected. Further, the wake width (see figure 4a), defined by the location where wake velocity reaching 95% of freestream [13], appears to be inversely proportional to the yaw angle as a result of reduction in rotor swept area normal to the inflow. This comparison was not possible at larger downstream distances

(represented in figure 4b-d) since the measurement field of view did not cover the entire wake region for all the yaw cases.

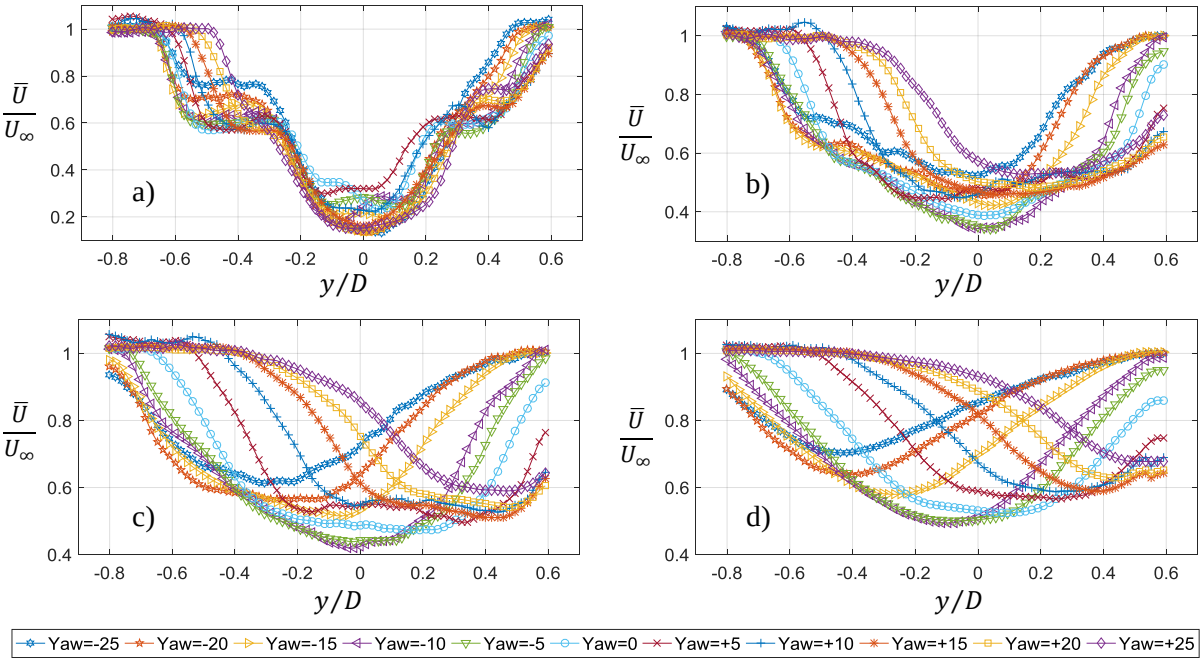

Figure 4. Normalized mean streamwise velocity ($\bar{U}/U_\infty$) profiles in the horizontal plane at hub height for different yaw angles. a) x/D=1, b) x/D=3, c) x/D=5, d) x/D=7.

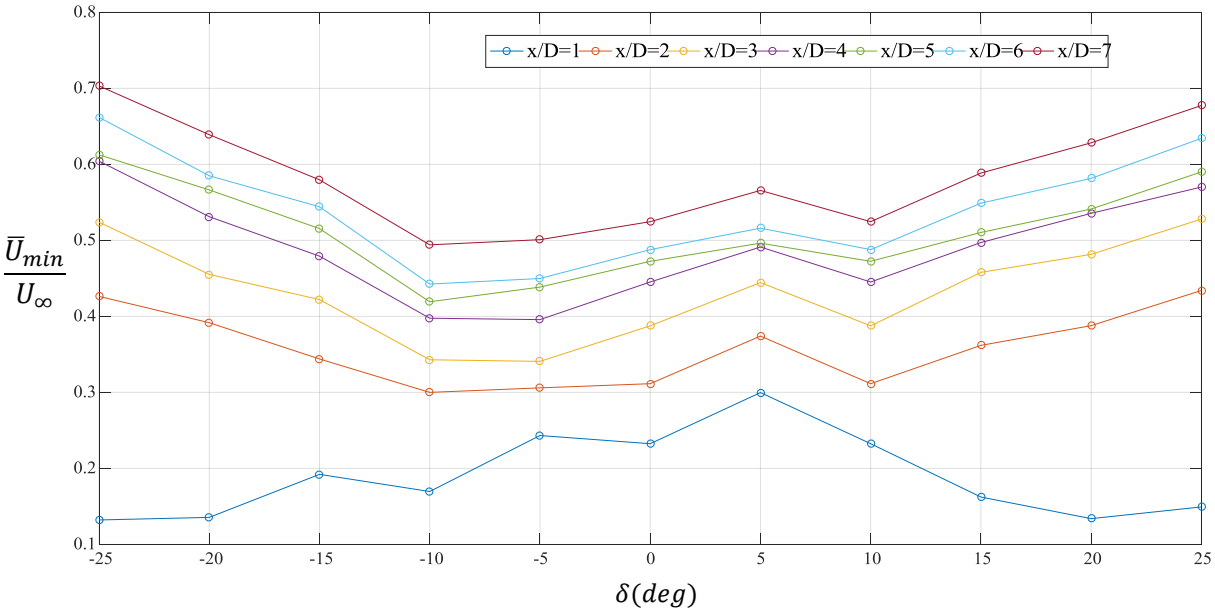

Figure 5. Normalized minimum mean streamwise velocity ($\bar{U}_{min}/U_\infty$) as a function of δ.

The wake center (y_c/D) is the cross stream location of the minimum mean streamwise wake velocity ($\bar{U}_{min}/U_\infty$) [14], is of importance in wake deflection analysis. Its deviation from the predominant flow direction is regarded as a measure of the wake deflection (y_c/D). Therefore, in subsequent analysis the variation of $\bar{U}_{min}/U_\infty$ with δ and x/D is considered.

Figure 5 plots $\overline{U}_{min}/U_\infty$ as a function of δ for different downstream distances. It was observed that for |δ|>15, and x/D>1, $\overline{U}_{min}/U_\infty$ increases with δ. Further, for |δ|<15°, the minimum $\overline{U}_{min}/U_\infty$ is sensitive to yaw angle direction. The cause for this pronounced asymmetry is under investigation. However, for wake deflection analysis, y/D is independent of the magnitude of $\overline{U}_{min}/U_\infty$ and is not considered further for this study.

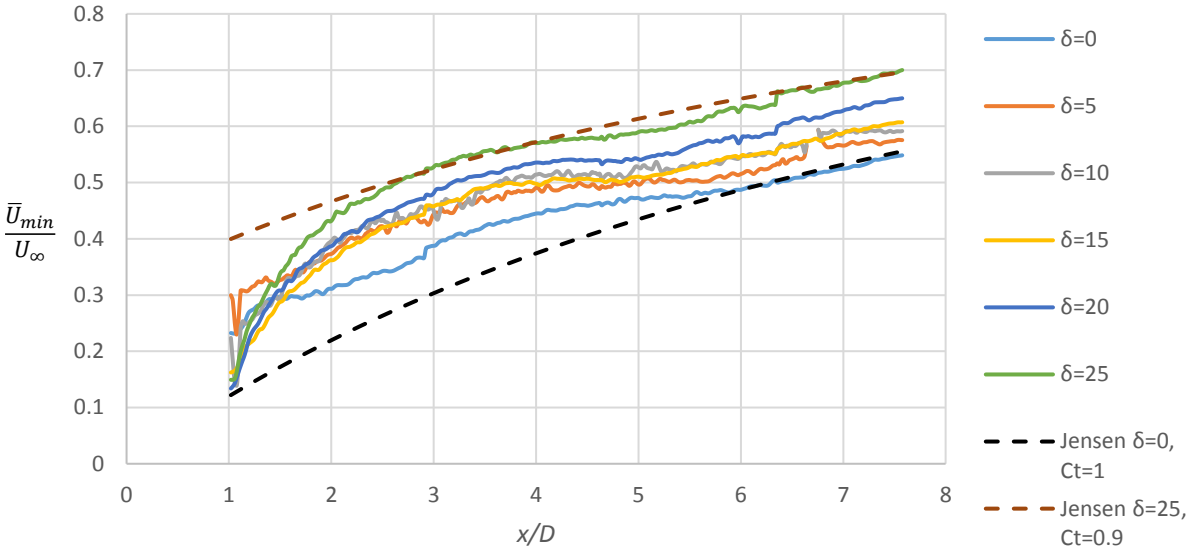

Figure 6. $\overline{U}_{min}/U_\infty$ as a function of the downstream distance for different positive yaw angles.

Figure 6 plots $\overline{U}_{min}/U_\infty$ as a function of the downstream distance for different positive yaw angles. As the wake progresses downstream, $\overline{U}_{min}/U_\infty$ increases as expected. However, $\overline{U}_{min}/U_\infty$ is also proportional to δ at various downstream distances. This observation could be explained by understanding the variation of thrust coefficient (C_T) with δ. Since in these experiments C_T was not directly measured, C_T was estimated by comparing the measured $\overline{U}_{min}/U_\infty$ with far wake velocity model proposed by Jensen [15],

$$\frac{U}{U_\infty} = 1 - \frac{1-\sqrt{1-C_T}}{\left(1+2k\frac{x}{D}\right)} \qquad (2)$$

Figure 6 also plots model estimated $\overline{U}_{min}/U_\infty$ as a function of the downstream distance for δ=0° and C_T =1 and for δ=25° and C_T = 0.9. In both cases k=0.033 is assumed. The C_T values were selected since their corresponding Jensen model curves appear to be the best fit to the measured $\overline{U}_{min}/U_\infty$ data in the far wake. Therefore, figure 6 implies that C_T is inversely proportional to δ, explaining the proportionality between $\overline{U}_{min}/U_\infty$ and δ. In our future experiments, direct C_T measurements will be made to explain observations with more certainty.

Figure 7 plots y_c/D, the location of the measured $\overline{U}_{min}/U_\infty$ for different yaw angles compared to outcomes from different wake simulation models, NREL 5MW reference SOWFA simulations [7], DTU CFD simulation [1], Qblade simulations of a Vestas V27 turbine, a wind tunnel study from NTU [2], and a full scale study from Sandia CREW project (1.5 years average observations on 67 x 1.5 MW turbine in the mid-West) [10]. As the turbine was yawed from 0° to 25°, it was assumed to be operating with a C_T value between 0.9 to 1, which is valid in the far wake. For comparison purposes, all data shown in figure 7 were scaled linearly to C_T~1 and x/D~7 according to the DTU linear model proposed by Guntur et. al [1]:

$$\frac{y_c}{D} = 0.24\,\frac{x}{D}\,C_T\,tan(\delta) \qquad (3)$$

The HAWKS measured y_c/D is in agreement with the Guntur model (with exception of deviation at higher δ and x/D), and results from other wake models, wind tunnel and full scale studies. The agreement of preliminary results implies that the scaled HAWKS platform can predict wake deflection observed in various studies which include the full scale tests, and is therefore appropriate for validating wake control strategies to be implemented in full scales wind farms.

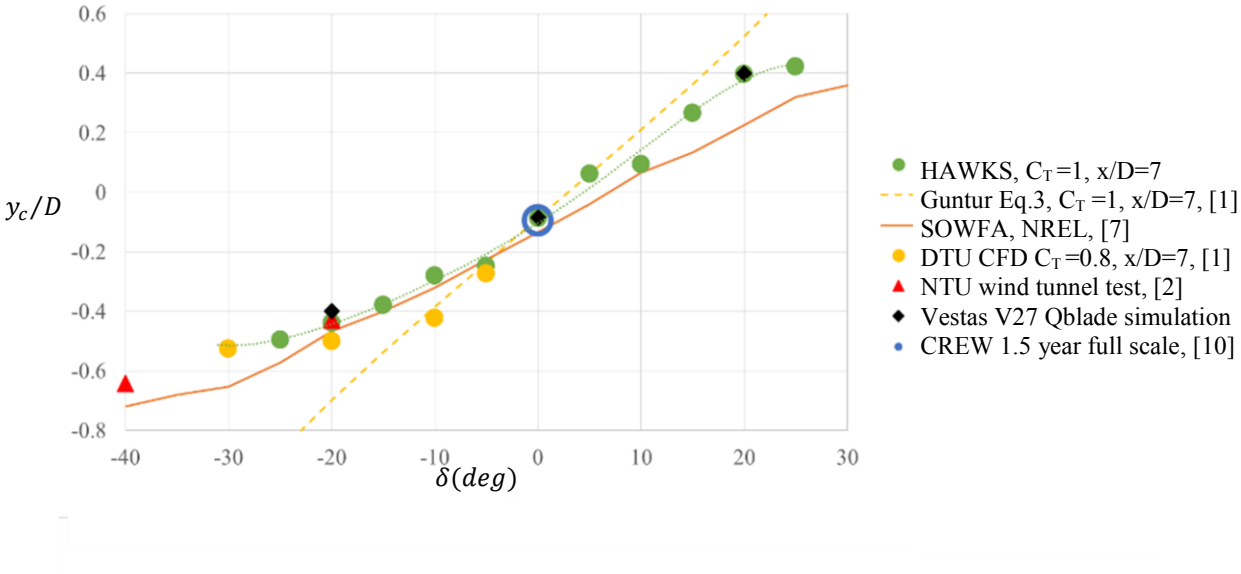

Figure 7. Comparison of the HAWKS results with different previous studies.

3.3. Wake characteristics under dynamic yaw

Full scale turbines are influenced by yaw misalignment due the inherent variability in the inflow or incorrect wind direction measurement obtained from nacelle mounted anemometers [1]. As it was shown in the previous sections, the yawed turbine performs at a lower C_P and C_T. Therefore, to reproduce an oscillating incident wind, a servomotor was adapted to the tower base to apply variable yaw angle. The eventual objective is to demonstrate the possibility of instantaneously controlling the yaw angle to steer the wake dynamically. As an initial trial, a test was performed at a fixed yaw rate of 2.5°/sec from -20° to 20°. The resulting contours of the instantaneous streamwise velocity (U/U_∞) are presented in figure 8. The problem of damaged pixels observed in figure 3 was rectified by enhancing the tracer particle density and reducing the light sheet thickness at these locations. Although this resulted in an increase in light sheet thickness at other locations, the measurement quality improved overall. The [instantaneous] contours show clearly the wake deflection as the yaw angle changes dynamically and also the turbulent nature of the wake. The arrows show the chronological direction of the wake deflection as the yaw angle changes. The implication of the dynamic yaw on the previously stated wake deflection test are yet to be estimated.

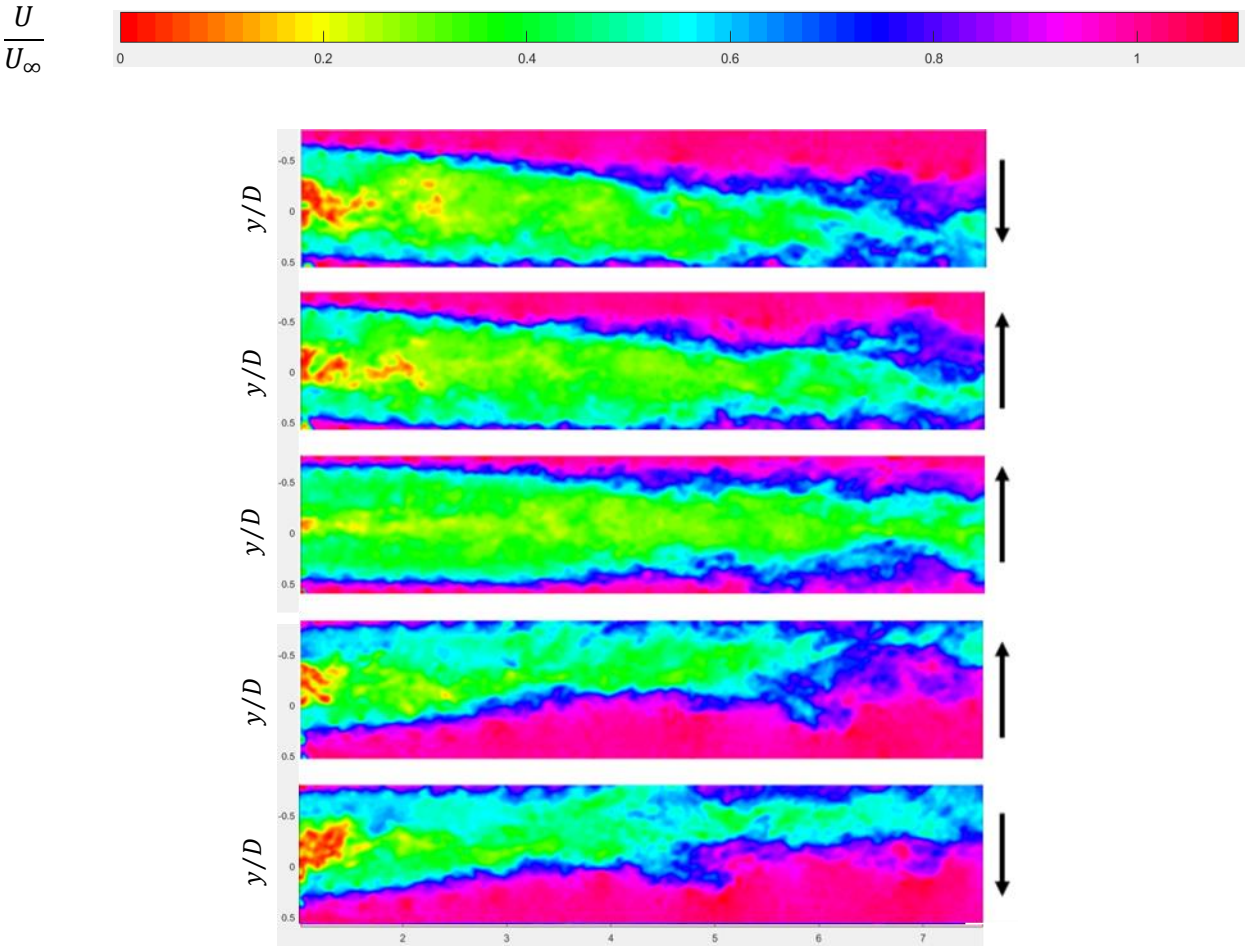

Figure 8. Contours of the instantaneous normalized stream wise velocity ($\overline{U}/U_\infty$) in the horizontal plane at hub height.

4. Conclusion and Future work

The HAWKS platform capabilities were introduced and the preliminary design was completed and tested. The tests demonstrated the wake steering for static and dynamic yaw. The measured wake deflections for static yaw are in agreement with previous wake models and field study, implying the clear applicability of scaled platforms such as HAWKS to research wake control strategies for full scale cases. The results obtained so far have helped identifying potential improvements in turbine design and modification in the experimental setup, which will be carried out in the near future.

Improvements in the mechanical design of turbine, particularly to reduce the influence of the nacelle, pitch accuracy and blade design will be performed before proceeding to turbine mass production. Modifications to the experimental setup will include relocation of the turbine hub in the middle of the tunnel cross section, increasing the field of view to cover a larger extension of the wake as the field of view of the current setup does not cover an acceptable area to properly characterize the wake, especially at high yaw angles. In addition, the wake deflection as the yaw angle changes has been demonstrated. However, the effect of changing C_T in the wake performance needs to be determined. Therefore, the capability to measure C_T will be added to the future experimental setup.

References

[1] S. Guntur, N. Troldborg, and M. Gaunaa, "Application of engineering models to predict wake deflection due to a tilted wind turbine," in *EWEA 2012-European Wind Energy Conference & Exhibition*, 2012.
[2] B. Andresen, "Wake behind a wind turbine operating in yaw," Master Thesis, Norwegian University of Science and Technology, 2013.
[3] M. Bastankhah and F. Porté-Agel, "A wind-tunnel investigation of wind-turbine wakes in yawed conditions," in *Journal of Physics: Conference Series*, 2015, p. 012014.
[4] K. A. Kragh, M. H. Hansen, and T. Mikkelsen, "Precision and shortcomings of yaw error estimation using spinner-based light detection and ranging," *Wind Energy,* vol. 16, pp. 353-366, 2013.
[5] B. Neha Marathe, "Investigation of power performance and wakes of wind turbines under yawed flow," Texas Tech University, 2014.
[6] J. M. Obrecht, "Method and system for improving wind farm power production efficiency," ed: Google Patents, 2013.
[7] M. Churchfield, J. Michalakes, P. Spalart, and P. Moriarty, "Evaluating techniques for redirecting turbine wake using SOWFA," 2013.
[8] J. Annoni, P. Seiler, K. Johnson, P. Fleming, and P. Gebraad, "Evaluating wake models for wind farm control," in *American Control Conference (ACC), 2014*, 2014, pp. 2517-2523.
[9] S. L. Matt Churchfield, "NWTC Informational Portal (SOWFA)," 2015.
[10] S. Martin, C. Westergaard, and J. White, "Visualizing Wind Farm Wakes Using SCADA Data," Sandia National Laboratories 2016.
[11] S. N. Laboratories. *Scaled Wind Farm Technology (SWiFT)*. Available: http://energy.sandia.gov/energy/renewable-energy/wind-power/wind_plant_opt/
[12] P. Fleming, P. M. Gebraad, S. Lee, J. W. Wingerden, K. Johnson, M. Churchfield*, et al.*, "Simulation comparison of wake mitigation control strategies for a two-turbine case," *Wind Energy,* vol. 18, pp. 2135-2143, 2015.
[13] C. Tsalicoglou, "Numerical Study of Wind Turbine Wake Aerodynamics in Uniform and Yawed Inflow," Master Thesis ETH Zurich, 2012, 2012.
[14] H. Wang and R. Barthelmie, "Wind turbine wake detection with a single Doppler wind lidar," in *Journal of Physics: Conference Series*, 2015, p. 012017.
[15] I. Katic, J. Højstrup, and N. O. Jensen, "A simple model for cluster efficiency," in *European Wind Energy Association Conference and Exhibition*, 1986, pp. 407-410.